Eurasian Chem.-Technol. J. 27 (2025) 281–287
The journal of the Institute of Combustion Problems https://ect-journal.kz

https://doi.org/10.18321/ectj1675

Selective CO Evolution from CO_2 over Ag-Ni-Based Cocatalyst-Modified Perovskite under Simulated Solar Light

Aibol Baratov[1,2], Chingis Daulbayev[2], Zhengisbek Kuspanov[1,2]*

[1]Satbayev University, 22 Satbayev str., 050013, Almaty, Kazakhstan
[2]Institute of Nuclear Physics, 1 Ibragimov str., 050032 Almaty, Kazakhstan

Article info

Received:
27 July 2025

Received in revised form:
10 September 2025

Accepted:
15 October 2025

Keywords:
Dual cocatalyst photodeposition
Charge carrier separation
Al-STO photocatalyst
CO_2 photoreduction
CO selectivity

Abstract

Photocatalytic CO_2 reduction offers a dual benefit of mitigating greenhouse gas emissions while generating renewable fuels. In this study, a composite photocatalyst based on aluminum-doped strontium titanate (Al-STO) was synthesized via a flux method and modified with dual cocatalysts: metallic Ag (reductive site) and a Ni-based species (oxidative site). Sequential photodeposition enabled precise loading, yielding a catalyst with enhanced charge separation and suppressed recombination. Structural and spectroscopic analyses confirmed the uniform dispersion of cocatalysts and broadened light absorption into the visible range. Photocatalytic evaluation under simulated solar light revealed a more than twofold increase in CO production (24.2 $\mu mol \cdot g^{-1} \cdot h^{-1}$) and high selectivity (up to 99%), compared to pristine Al-STO. The observed performance enhancement is attributed to the synergistic interaction between Ag and the Ni-based cocatalyst, enabling spatially resolved charge carrier pathways. These results highlight the promise of cocatalyst engineering on perovskite surfaces for selective CO_2-to-fuel conversion under solar irradiation.

1. Introduction

Over the past century, industrialization has significantly improved quality of life but has also led to the intensive exploitation of natural resources and increased anthropogenic pressure on the environment [1, 2]. This has resulted in large-scale emissions of pollutants – ranging from organic and inorganic compounds to CO_2, nanoparticles, and radioactive isotopes – that pose serious risks to human health and environmental sustainability [3, 4]. Of particular concern is the growing concentration of greenhouse gases, especially CO_2, which is highly chemically stable and can persist in the atmosphere for several hundred years [5, 6]. Even with a complete cessation of emissions, global warming would remain a long-term challenge. Under these circumstances, the development of effective CO_2 capture and conversion methods – including photocatalytic reduction – has become a top priority in contemporary science.

CO_2 capture and conversion are critical steps toward achieving sustainable development and carbon neutrality [7]. Amid escalating environmental pressures, the development of safe and efficient technologies for converting CO_2 into high-value-added products has gained particular relevance [8]. Among these, photocatalytic reduction is especially promising, as it uses solar energy to convert CO_2 into valuable chemicals such as CO, CH_4, and CH_3OH [9]. This technology offers environmental friendliness, renewability, and the potential to simultaneously reduce carbon emissions and generate alternative fuels.

Among photocatalytic materials for CO_2 reduction, perovskites – particularly $SrTiO_3$ (STO) – stand out due to their high thermal and chemical stability and versatile crystal structure [10–12]. STO exhibits strong activity in reactions such as photocatalytic water splitting [13, 14]. However, its wide bandgap and inefficient charge separation limit its photocat-

*Corresponding author.
E-mail address: zhenis.kuspanov@gmail.com

alytic performance. Various strategies have been proposed to enhance the properties of STO, including the formation of heterojunctions with carbon quantum dots [15], cation doping with elements such as Ni and Al [16, 17] and modification with dual cocatalysts such as Ag and Co [18]. These approaches aim to enhance light absorption, suppress charge recombination, and improve overall photocatalytic efficiency.

In this study, we report the development of an Al-doped STO composite modified with dual cocatalysts (Ag and Ni), synthesized via a deposition method for the selective photocatalytic reduction of CO_2 to CO under simulated sunlight. Silver nanoparticles function as active sites for CO_2 reduction, while Ni-based cocatalyst serve as oxidation sites. The incorporation of dual cocatalysts enhances charge separation and stabilizes the photocatalytic process, as confirmed by structural, morphological, and catalytic analyses.

2. Experimental part

2.1. Materials

Titanium(IV) oxide, anatase (TiO_2, particle size <25 nm, 99.7%), strontium nitrate ($Sr(NO_3)_2$, ≥98%), aluminum oxide (Al_2O_3, particle size <50 nm, 99.8%), silver nitrate ($AgNO_3$, 99.8%), and sodium sulfate (Na_2SO_4) were purchased from Sigma–Aldrich (St. Louis, MO, USA). Nickel nitrate ($Ni(NO_3)_2$) was obtained from Laborpharma (Almaty, Kazakhstan), as well as strontium chloride hexahydrate ($SrCl_2 \cdot 6H_2O$, 99.7%). Titanium dioxide (TiO_2, anatase phase, 99.9%) and oxalic acid ($(COOH)_2$, purity >99%) were also acquired from MERYER. All chemicals were used without any additional treatment.

2.2. Synthesis of STO, Al-STO and Ag-Ni/Al-STO

STO nanoparticles were synthesized via a co-precipitation method followed by calcination, in accordance with previously reported procedures [19, 20]. Briefly, TiO_2 was introduced into an aqueous solution of $Sr(NO_3)_2$ at a Ti:Sr molar ratio of 1:1. The mixture was dispersed using ultrasound, followed by the addition of a 0.4 M oxalic acid solution at pH 6–7. The resulting precipitate was separated, washed, dried, and calcined at 1100 °C for 60 minutes. For Al doping, the obtained STO was mixed with Al_2O_3 and $SrCl_2$ (1:0.02:10 molar ratio) and thermally treated at 1150 °C for 10 hours. After cooling, the product was washed with deionized water and dried at 60 °C.

To prepare photocatalytic samples, 0.2 g of Al-doped STO powder was dispersed in 100 mL of distilled water using an ultrasonic bath. The suspension was then transferred to a glass photoreactor and irradiated with a 300 W xenon lamp under continuous stirring. For the synthesis of Ag/Al-STO, 208 µL of 0.1 M $AgNO_3$ was added and the mixture was irradiated for 60 minutes. The Ag-Ni/Al-STO sample was prepared sequentially: first, 104 µL of 0.1 M $AgNO_3$ was added and irradiated for 10 min, followed by the addition of 176 µL of 0.1 M $Ni(NO_3)_2$ and further irradiation for 50 minutes. The total cocatalyst loading was 3 wt.% relative to Al-STO, ensuring uniform dispersion and the formation of active sites.

2.3. Characterization

The morphology and elemental composition of the samples were examined by scanning electron microscopy (SEM, Zeiss Crossbeam 540, Germany) at an accelerating voltage of 5–20 kV. A high-resolution TEM (JEM-2100 LaB6 HRTEM, JEOL, Japan) operated at 80 kV was used to define the morphology of the samples. The phase composition was determined by X-ray diffraction (XRD) using a D8 ADVANCE diffractometer (Bruker, Germany) with Cu Kα radiation (λ = 1.5406 Å) operated at 40 kV and 40 mA, over a 2θ range of 10–80°. The surface chemical composition was analyzed by X-ray photoelectron spectroscopy (XPS, VG-Microtech Multilab 3000) using Mg/Al anodes. Optical properties were studied using UV-Vis diffuse reflectance spectroscopy (DRS) on an Agilent Cary 5000 spectrophotometer in the 200–800 nm wavelength range.

2.4. Photocatalytic reaction

Photocatalytic CO_2 reduction using Ag/Al-STO and Ag-Ni/Al-STO composites was performed under irradiation from a 300 W xenon lamp in a sealed stainless-steel reactor at 25 °C and atmospheric pressure. For each experiment, 0.1 g of the photocatalyst sample was dispersed in 200 mL of 0.1 M $NaHCO_3$ solution, with continuous CO_2 (99.999%) flow at a rate of 30 mL/min. Prior to illumination, the reactor was purged with high-purity CO_2 for 1 h to remove residual air and ensure complete saturation of the solution, followed by 1 h of irradiation under sealed conditions. The gaseous products (H_2, O_2, and CO) were analyzed using a CROMOS 1000 gas chromatograph equipped with TCD and FID detectors. The chromatograph was directly connected to the reactor, and gas sampling was conducted every hour. Argon was used as the carrier gas.

3. Results and Discussion

3.1. Sample characterization

3.1.1. SEM and TEM analysis

The morphological characteristics of the Ag/Al-STO and Ag-Ni/Al-STO samples were thoroughly investigated using SEM and TEM. The SEM images show cube-like Al-STO particles with slightly rounded edges, which is typical for materials subjected to high-temperature thermal treatment. Uniformly distributed Ag nanoparticles with an average size of 10–15 nm are clearly visible on the Al-STO surface (Fig. 1a,c), indicating a high degree of dispersion and the formation of a thin metallic coating that facilitates efficient electron transfer [21]. In the Ag-Ni/Al-STO sample (Fig. 1b,d), pronounced agglomeration of NiO_x is observed, accompanied by the formation of flake-like and plate-like structures. This morphology may be associated with the self-assembly behavior of Ni-based particles influenced by factors such as ion concentration, pH, and temperature, as described by Lee et al. [22]. According to this mechanism, Ni-based particles tend to form aggregated structures in the form of nanosheets or nanofibers through directional agglomeration [23].

These microscopy results confirm the successful and selective loading of Ag and Ni-based cocatalysts onto the Al-STO surface, which is critical for enhancing the efficiency of photocatalytic CO_2 reduction.

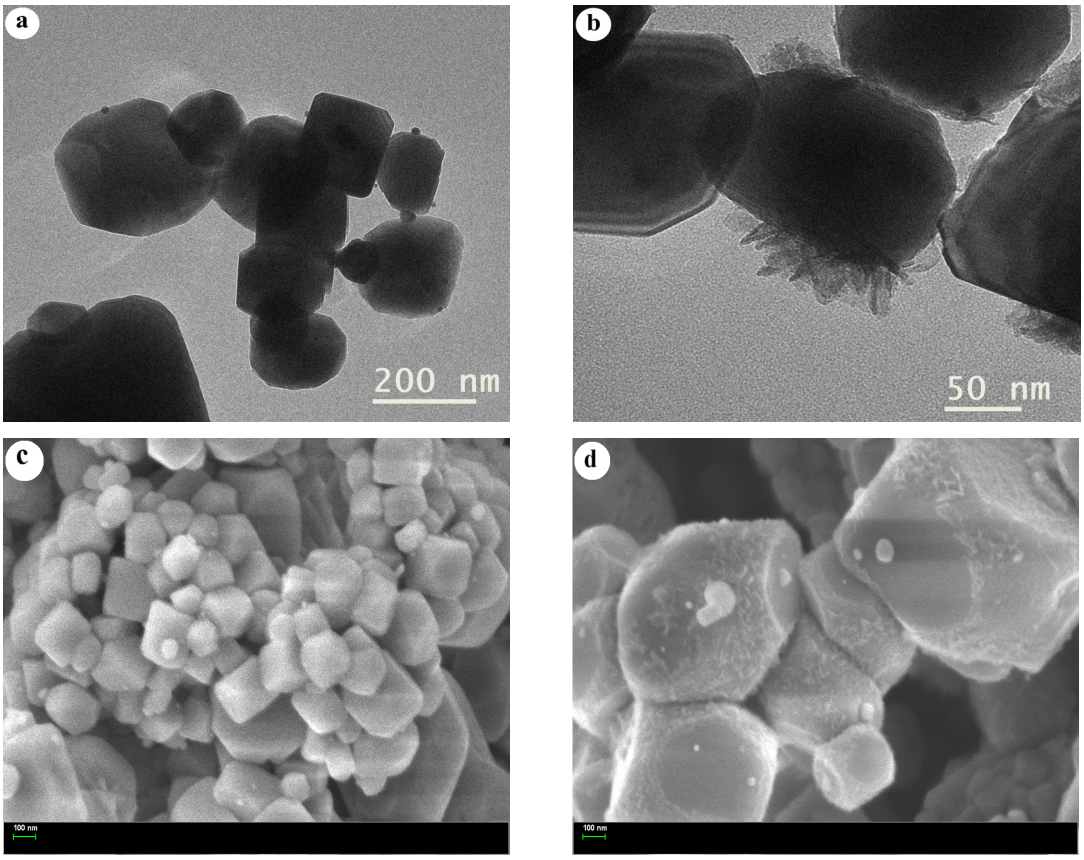

Fig. 1. (a, b) TEM and (c, d) SEM images of the obtained samples: (a, c) – Ag/Al-STO; (b, d) – Ag-Ni/Al-STO.

3.1.2. XRD, UV-Vis DRS, XPS

XRD analysis (Fig. 2a) confirmed that the modification of Al-STO with Ag and NiO_x does not alter its crystal structure. All diffraction peaks correspond to the perovskite phase of STO with cubic symmetry (space group Pm-3m, ICSD 23076), indicating that the original lattice is preserved even after cocatalyst deposition. No distinct peaks related to Ag or Ni phases were detected, likely due to their high dispersion and low surface concentration.

To further clarify the chemical states of the elements and verify the successful loading of Ag-Ni cocatalysts, XPS analysis of the Ag-Ni/Al-STO sample was conducted. The high-resolution Ag 3d spectra (Fig. 2b) show two characteristic peaks at binding energies of 368.25 and 374.17 eV, corresponding to Ag $3d_5/_2$ and Ag $3d_3/_2$, respectively, which are typical of metallic silver (Ag^0), although the possible presence of Ag_2O cannot be completely excluded. The high-resolution Ni 2p spectrum (Fig. 2c) exhibits signals around 855.8–856.0 eV (Ni $2p_3/_2$) along with

associated satellite peaks, which may correspond to Ni^{2+} species in $Ni(OH)_2$, NiO, or mixed NiO_x/Ag_2NiO_2 phases [24]. The coexistence of these nickel-containing species indicates their potential function as active sites that facilitate charge separation and transfer.

The optical properties of the materials were evaluated using UV–Vis diffuse reflectance spectroscopy (Fig. 2d). Upon cocatalyst loading, an enhancement of light absorption in the visible range was observed, indicating improved optical response. The absorption edge remained nearly unchanged compared to pristine Al-STO, confirming that the modification is surface-limited and does not interfere with the crystal lattice. The bandgap of Al-STO was estimated to be ~3.2 eV, consistent with literature data [25]. Based on the Tauc plot analysis (Fig. 2e), a slight narrowing of the bandgap was observed after Ag and NiO_x deposition, which may enhance visible-light absorption and contribute to the improved photocatalytic performance of the composite.

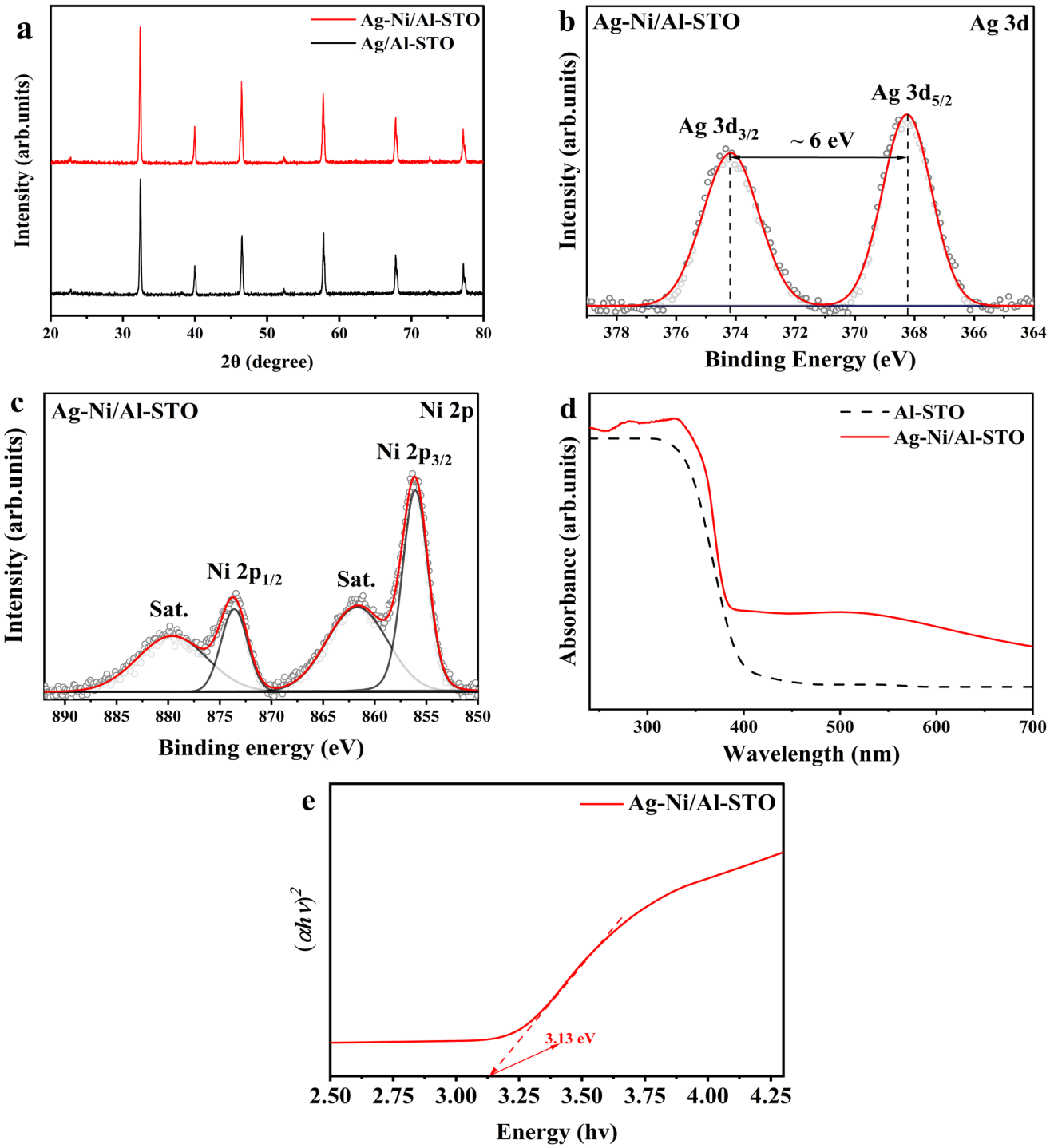

Fig. 2. (a) – XRD; XPS spectra: (b) – Ag 3d of Ag-Ni/Al-STO, (c) – Ni 2p of Ag-Ni/Al-STO; (d) UV-Vis absorption spectrum and (e) – Tauc's plot of the obtained photocatalysts.

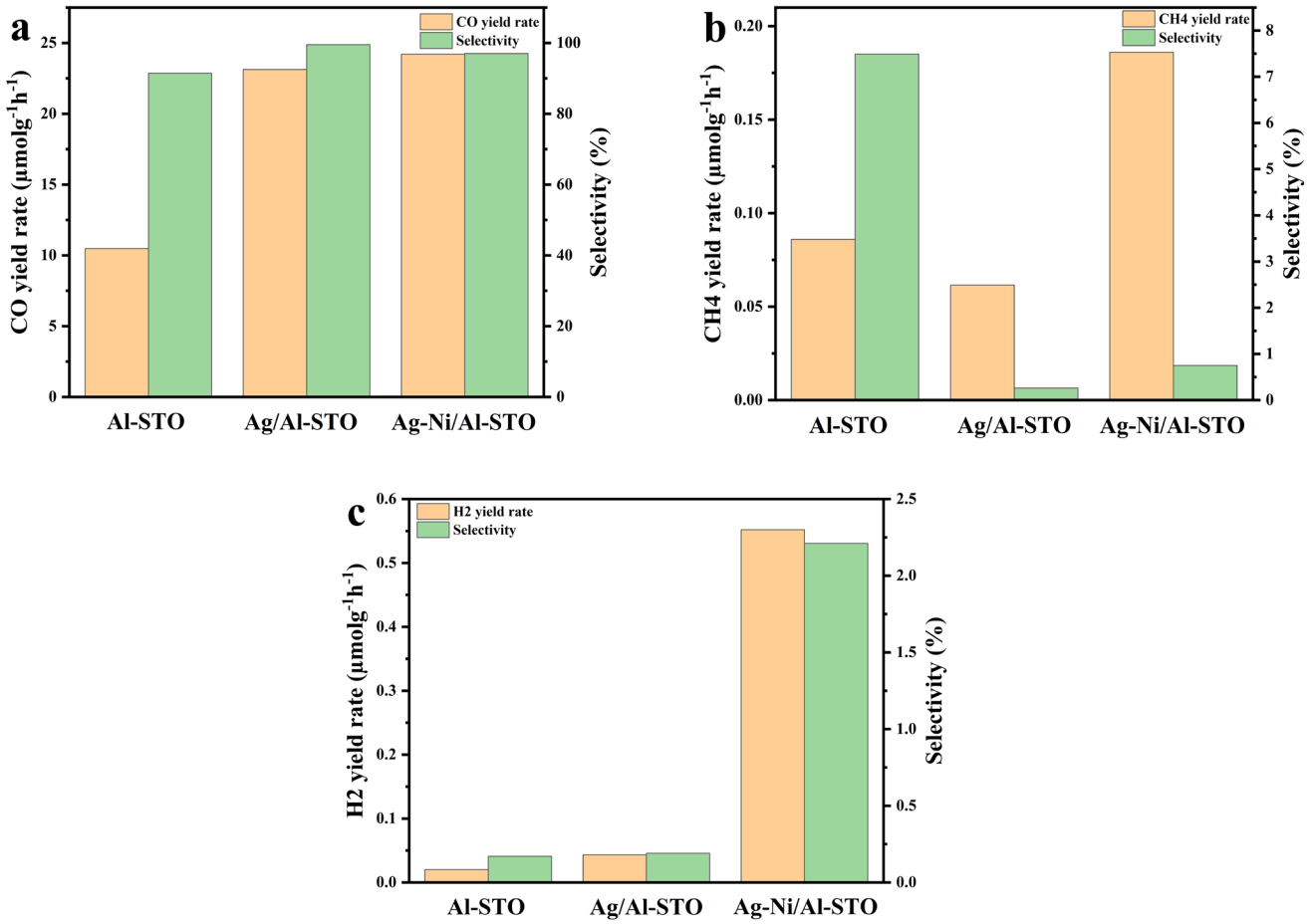

Fig. 3. Product yield (μmol·g^{-1}·h^{-1}) during photocatalytic reduction of CO_2 using synthesized photocatalysts: (a) – CO, (b) – CH_4, (c) – H_2.

3.2. Photocatalytic CO_2 reduction performance

The photocatalytic performance of the synthesized materials was systematically assessed through gas-phase CO_2 reduction under simulated solar irradiation. CO was targeted as the primary reduction product, while H_2, CH_4, and C_2H_6 were monitored as secondary by-products to evaluate selectivity and reaction pathways.

The bare Al-STO exhibited limited CO evolution, reaching 10.48 μmol·g^{-1}·h^{-1} with a selectivity of 91.47%, indicating moderate intrinsic activity and charge separation ability. Upon surface modification with plasmonic silver nanoparticles (Ag/Al-STO), the CO production rate more than doubled to 23.12 μmol·g^{-1}·h^{-1}, alongside a marked enhancement in selectivity to 99.51%. This improvement can be attributed to the efficient role of Ag as an electron sink, which promotes selective CO_2 reduction over competing H^+ reduction pathways, thereby suppressing side reactions yielding CH_4 (0.0615 μmol·g^{-1}·h^{-1}) and H_2 (0.0431 μmol·g^{-1}·h^{-1}).

Further introduction of a nickel-based oxidative cocatalyst (NiO_x) onto the Ag/Al-STO surface (Ag-Ni/Al-STO) yielded the highest CO evolution rate of 24.2 μmol·g^{-1}·h^{-1}, reflecting enhanced charge carrier generation and separation. However, this came at the expense of selectivity, which decreased to 96.99% due to a concurrent increase in H_2 (0.552 μmol·g^{-1}·h^{-1}) and CH_4 (0.186 μmol·g^{-1}·h^{-1}) evolution. This suggests that while the dual cocatalyst system synergistically boosts the overall photocatalytic activity by facilitating charge extraction from both the conduction and valence bands, it also introduces additional reduction pathways, leading to partial loss of CO_2 reduction specificity.

In summary, Ag nanoparticles play a pivotal role in enhancing CO selectivity via efficient electron trapping and transfer, whereas the combination of Ag and Ni-based cocatalysts significantly elevates total CO_2 conversion rates. Therefore, Ag/Al-STO is optimal for selective CO generation, while Ag-Ni/Al-STO maximizes overall photocatalytic activity, highlighting the trade-off between selectivity and productivity in dual-cocatalyst systems.

4. Conclusions

In this study, STO doped with aluminum (Al-STO) was modified with dual cocatalysts – Ag and Ni – via sequential photodeposition to improve photocatalytic CO_2 reduction. Structural and surface characterization (XRD, XPS, SEM, TEM) confirmed successful and selective deposition of cocatalysts without phase contamination or lattice distortion. The Ag nanoparticles served as effective reduction sites, facilitating selective electron transfer to CO_2, while the Ni-based cocatalyst promoted hole transfer and oxidation reactions. UV-Vis DRS analysis revealed enhanced visible-light absorption, attributed to the surface plasmon resonance (SPR) of Ag and light-harvesting by Ni-based.

Photocatalytic tests under simulated sunlight demonstrated that the dual-cocatalyst system significantly outperformed the unmodified Al-STO in terms of CO evolution rate and selectivity. Specifically, Ag/Al-STO exhibited the highest CO selectivity (99.51%), while Ag-Ni/Al-STO achieved the highest CO production rate (24.2 $\mu mol \cdot g^{-1} \cdot h^{-1}$), indicating a synergistic interaction between reductive and oxidative sites. The enhanced performance is attributed to improved charge separation and reduced recombination within the heterostructure.

These findings highlight the importance of spatially resolved cocatalyst design in achieving efficient and selective CO_2 conversion. The Ag–Ni/Al-STO system represents a promising photocatalyst for sustainable CO_2-to-fuel conversion under solar irradiation.

Acknowledgments

This research has been funded by the Science Committee of the Ministry of Science and Higher Education of the Republic of Kazakhstan (Grant No BR24992935).

References

[1]. F.A. Rahman, M.M.A. Aziz, R. Saidur, et al., Pollution to solution: Capture and sequestration of carbon dioxide (CO2) and its utilization as a renewable energy source for a sustainable future, *Renew. Sustain. Energy Rev.* 71 (2017) 112–126. DOI: 10.1016/j.rser.2017.01.011

[2]. S. Talishinskaya-Abbasova, J.I. Mikayilov, Impact of financial development on carbon dioxide emissions: empirical evidence from Azerbaijan, Russia, and Kazakhstan, *Environ. Econ. Policy Stud.* (2024). DOI: 10.1007/s10018-024-00415-2

[3]. E. Cipriani, A. Gemignani, D. Menicucci, Awareness of everyday effects of climate change: The climate change perceptual awareness scale (CCPAS), *Heliyon* 10 (2024) e38461. DOI: 10.1016/j.heliyon.2024.e38461

[4]. G. Fadillah, T.A. Saleh, Advances in mesoporous material for adsorption and photoconversion of CO_2 in environmental pollution: Clean environment and clean energy, *Sustain. Chem. Pharm.* 29 (2022) 100812. DOI: 10.1016/j.scp.2022.100812

[5]. C.H. Lim, B.S. Lim, A.R. Kim, et al., Chapter 7 - Climate change adaptation through ecological restoration, in: M.K. Jhariya, R.S. Meena, A. Banerjee, S.N. Meena (Eds.), Natural Resources Conservation and Advances for Sustainability, 2022, pp. 151–172. DOI: 10.1016/B978-0-12-822976-7.00013-2

[6]. N. Saitova, K. Askaruly, N. Idrissov, et al., MXene-Integrated Porous Carbon–Silicon Composite as a Stable and High-Capacity Anode for Lithium-Ion Batteries, *Eng. Sci. 37* (2025). DOI: 10.30919/es1804

[7]. F. Wang, J.D. Harindintwali, Z. Yuan, et al., Technologies and perspectives for achieving carbon neutrality, *Innovation* 2 (2021) 100180. DOI: 10.1016/j.xinn.2021.100180

[8]. C. Feng, T. Lin, R. Zhu, et al., Key technologies for CO_2 capture and recycling after combustion: CO_2 enrichment in oxygen enriched combustion of converter gas, *J. Clean. Prod*. 380 (2022) 135128. DOI: 10.1016/j.jclepro.2022.135128

[9]. A.R.A. Astuti, D. Ariono, I.G. Wenten, et al., Mechanistic insights into CO_2 photoreduction to formic acid using ZnO catalysts, *Chem. Eng. Res. Des.* 218 (2025) 664–673. DOI: 10.1016/j.cherd.2025.05.011

[10]. B. Boga, N.G. Moustakas, Y. Han, et al., Design of $SrTiO_3$-based catalysts for photocatalytic CO_2 reduction, *Catal. Sci. Technol.* 14 (2024) 3459–3472. DOI: 10.1039/D4CY00313F

[11]. J. Lei, W. Bi, M. Wang, et al., Efficient electron transport at the perovskite nanodots interface facilitates CO_2 photoreduction, *J. Colloid Interface Sci.* 679 (2025) 420–429. DOI: 10.1016/j.jcis.2024.09.179

[12]. J. Zhang, C. Qiu, L. Wang, et al., Inducing Cu^{2+} species to $SrTiO_3$ nanofibers based on blend electrospinning for boosting CO_2 photoreduction to CH_3OH, Ceram. Int. 50 (2024) 39374–39381. DOI: 10.1016/j.ceramint.2024.07.311

[13]. L. Chen, C. Wang, Z. Wang, G. Li, Pivotal role of water vapor–mediated defect engineering on $SrTiO_3$ nanofiber toward efficient photocatalytic

water splitting, *Mater. Today Energy* 44 (2024) 101622. DOI: 10.1016/j.mtener.2024.101622

[14]. A. Baratov, A. Dikov, L. Dikova, et al., $Srtio_3$-Based Composites for Photocatalytic Panels in Solar Hydrogen Production, *Molecules* 30 (2025) 3699. DOI: 10.3390/molecules30183699

[15]. Q. Wang, Y. Yuan, C. Li, et al., Carbon quantum dot-modified $TiO_2/SrTiO_3$ heterojunction for boosting photocatalytic CO_2 reduction, *Renew. Energy* 231 (2024) 120997. DOI: 10.1016/j.renene.2024.120997

[16]. H. Li, Y. Tang, W. Yan, et al., Vacancy-enhanced photothermal activation for CO_2 methanation on $Ni/SrTiO_3$ catalysts, *Appl. Catal. B Environ. Energy* 357 (2024) 124346. DOI: 10.1016/j.apcatb.2024.124346

[17]. A.K. Sahu, M. Pokhriyal, D. Banerjee, et al., An indirect Z-scheme heterostructure of nano-gold layer immobilized Cu-Al-doped $SrTiO_3$ and CoO_x-WO_3 for photocatalytic CO_2 reduction, *Chem. Eng. J.* 487 (2024) 150716. DOI: 10.1016/j.cej.2024.150716

[18]. Z. Kuspanov, A. Serik, N. Matsko, et al., Efficient photocatalytic degradation of methylene blue via synergistic dual co-catalyst on $SrTiO_3$@Al under visible light: Experimental and DFT study, *J. Taiwan Inst. Chem. Eng.* 165 (2024) 105806. DOI: 10.1016/j.jtice.2024.105806

[19]. S. Wang, K. Teramura, T. Hisatomi, et al., Dual Ag/Co cocatalyst synergism for the highly effective photocatalytic conversion of CO_2 by H_2O over Al-$SrTiO_3$, *Chem. Sci.* 12 (2021) 4940–4948. DOI: 10.1039/D1SC00206F

[20]. U. Abdikarimova, A. Serik, D. Yessenkeldina, et al., Impact of fabrication method on the photocatalytic efficiency of PAN/$SRTIO_3$@AL composite nanofibers, *J. Water Process Eng.* 78 (2025) 108803. DOI: 10.1016/j.jwpe.2025.108803

[21]. D. Kanakaraju, F.D. anak Kutiang, Y.C. Lim, P.S. Goh, Recent progress of Ag/TiO_2 photocatalyst for wastewater treatment: Doping, co-doping, and green materials functionalization, *Appl. Mater. Today* 27 (2022) 101500. DOI: 10.1016/j.apmt.2022.101500

[22]. W. Li, J. Yang, T.T. Isimjan, et al., Aqueous synthesis and growth of morphologically controllable, hierarchical $Ni(OH)_2$ nanostructures, *Mater. Res. Express* 2 (2015) 075011. DOI: 10.1088/2053-1591/2/7/075011

[23]. M. Cheng, H. Fan, Y. Song, et al., Interconnected hierarchical $NiCo_2O_4$ microspheres as high-performance electrode materials for super-capacitors, *Dalton Trans.* 46 (2017) 9201–9209. DOI: 10.1039/C7DT01289F

[24]. B. Laïk, M. Richet, N. Emery, et al., XPS Investigation of Co–Ni Oxidized Compounds Surface Using Peak-On-Satellite Ratio. Application to $Co_{20}Ni_{80}$ Passive Layer Structure and Composition, *ACS Omega* 9 (2024) 40707–40722. DOI: 10.1021/acsomega.4c05082

[25]. K. Aravinthkumar, E. Praveen, A. Jacquline Regina Mary, C. Raja Mohan, Investigation on $SrTiO_3$ nanoparticles as a photocatalyst for enhanced photocatalytic activity and photovoltaic applications, *Inorg. Chem. Commun*. 140 (2022) 109451. DOI: 10.1016/j.inoche.2022.109451